Analysis of Steric Hindrance Effects on Adsorption Kinetics and Equilibria

Xuezhi Jin, Julian Talbot, and N.-H. Linda Wang
School of Chemical Engineering, Purdue University, West Lafayette, IN 47907

Most existing adsorption models do not properly consider steric hindrance effects of preadsorbed solutes. As a consequence, the models often fail to represent the adsorption kinetics and equilibria accurately. In this work, we extend the random sequential adsorption concept for irreversible adsorption to analyze reversible adsorption on a continuous surface and a random site surface. Based on simulation results of these processes, general kinetic equations for one-component adsorption are developed. The equations are used to correlate chromatography frontal curves of lysozyme and isotherm data of ethane adsorption on activated carbon and ethylene adsorption on a molecular sieve. The significance of the equations, as compared with the Langmuir equation, lies not only in their ability to correlate the experimental data more accurately, but in the physical significance of the adsorption parameters such as the maximum adsorption capacity obtained from the correlation. Our study shows that steric hindrance effects alone result in nonlinear Scatchard and Hill plots with negative cooperativity.

Introduction

Adsorption, which involves preferential concentration of solute(s) at a liquid/solid or gas/solid interface, is of great interest in various fields of science and engineering. For example, by virtue of its high selectivity, adsorption chromatography is widely used for analysis of complex mixtures and for separation and purification of chemicals and biochemicals (Scope, 1982; Regnier, 1983; Wankat, 1990). Adsorption is also one of the crucial steps in heterogeneous catalysis, which is used in the manufacture of about 50% of the products in the chemical industry (Ben-Avraham, 1990). Understanding the rate of adsorption and the approach to equilibrium is a key issue in many engineering applications.

Many adsorption models, primarily for equilibrium isotherms, have been proposed. The most frequently used ones are the Langmuir model (Langmuir, 1918) and its various modified forms (Markham and Benton, 1931; Fowler and Guggenhein, 1939; Fritz and Schlunder, 1974), the Freundlich equation (Freundlich, 1926), the BET equation (Brunauer et al., 1939), the IAS (ideal adsorbed solution) model (Myers and Prausnitz, 1965; Glessner and Myers, 1969; Radke and Prausnitz, 1972) and the SDM (stoichiometric displacement model) (Kopaciewicz et al., 1983; Rounds and Regnier, 1984). All these have a common limitation, that is, none of them properly takes into account the steric hindrance (blocking) effects of the preadsorbed solutes.

In contrast to the large number of available isotherm equations, very few intrinsic kinetic equations have been proposed or verified. This may be in part due to the difficulties in obtaining accurate experimental kinetic data, although various optical techniques have been developed to measure the adsorption rate for single component systems (Cuypers, 1976; Kop et al., 1984; Leininger et al., 1984; Tiefenthaler and Lukosz, 1989; Ramsden,1992).

The most widely used kinetic equation is that due to Langmuir (1918):

$$\frac{d\theta^*}{dt} = k_a c(1-\theta^*) - k_d\theta^* \tag{1}$$

where $\theta^* = q/q_m$ is the fractional amount adsorbed, q is the amount adsorbed per unit mass or volume of adsorbent, and q_m is the maximum adsorption capacity. The symbols t, c, k_a, and k_d have their conventional meanings, that is, adsorption time, solute concentration in the solution directly in contact with the surface, and adsorption and desorption rate constants, respectively.

This model is based on the assumption that, the adsorption site density, ρ_{site}, is so low that the average distance between two adjacent sites is larger than the solute diameter. Thus, provided the solutes adsorb centered on the sites, the occupation of a site by a solute will not affect the accessibility of any other sites by new solutes. In this case, clearly, $q_m = \rho_{site}$ and the fraction of available sites is simply by $1-\theta^*$.

We argue that these assumptions are invalid in many adsorption processes, particularly those involving the adsorption of large molecules on a surface with high ρ_{site}. In this case, the occupation of a site will exclude some other sites from further occupation, and steric hindrance effects become significant. Therefore, the simple Langmuir model is inadequate for describing the adsorption kinetics and equilibrium isotherm (which is just a special case of the former). A good example is the inability of the model to correlate accurately the breakthrough curves of proteins (Skidmore et al., 1990; Mao et al., 1991).

To illustrate the concept of steric hindrance, we introduce the following model. The solutes are represented as hard spherical particles of diameter σ, while the adsorbent is a planar surface of area L^2 onto which a number, N_{site}, of adsorption sites have been distributed at random. Consider a typical adsorption configuration, as shown in Figure 1. The shaded area represents the union of the exclusion circles, each of diameter 2σ, of all adsorbed particles. Any site lying within this area cannot be occupied by an additional solute, since this would result in overlap with preadsorbed solutes. Only those sites lying within the white (unshaded) areas are available. It is evident that the fraction of available sites, which we denote by ϕ, is no longer simply related to the coverage by $1-\theta^*$. To account for steric blockage, a generalized Langmuir equation can be used, in which the $(1-\theta^*)$ term in Eq. 1 is replaced by the function ϕ:

$$\frac{d\theta^*}{dt} = k_a c\phi - k_d\theta^* \tag{2}$$

The concept of ϕ was first introduced by Widom (1966) for irreversible adsorption on a continuous surface (CS), on which a solute may adsorb in any location (in this case, ϕ is known as the available surface function). The CS is an appropriate model for hydrophobic adsorption surface, onto which solutes bind via nonspecific hydrophobic interactions.

When exclusion effects are significant, ϕ depends on the way that the particles are introduced into the surface. One method, corresponding to an irreversible adsorption process, is to use the random sequential adsorption (RSA) algorithm: (1) the center of a solute is placed at a randomly selected position (or site) on the surface; (2) if the trial solute does not overlap with any of preadsorbed solutes, it is fixed permanently in this position (or site); and (3) otherwise it is rejected. If the trials are continued, the surface approaches a saturated state (the "jamming limit") in which no position (or site) on the surface is available.

The RSA of various systems, both on lattices and continuous substrates has been studied by numerous investigators, primarily from an applied mathematics/theoretical physics viewpoint (Bartelt and Privman, 1991; Evans, 1993). However, some attempts have been made to apply the model to the irreversible adsorption of proteins (Feder et al., 1980a), latex spheres (Onoda and Liniger, 1986), and colloids (Adamczyk et al., 1983; Privman et al., 1991). We note in particular the recent work of Ramsden (1993) who studied the adsorption kinetics of transfer in on a planar $Ti_xSi_{1-x}O_2$ ($x \approx 0.3$) surface with an optical waveguide technique. He attempted to verify the series expansion of ϕ for low to intermediate coverages (Schaaf and Talbot, 1989a), and the asymptotic behavior at high coverage (Feder, 1980b; Pomeau, 1980; Swendson, 1981) in RSA in two dimensions.

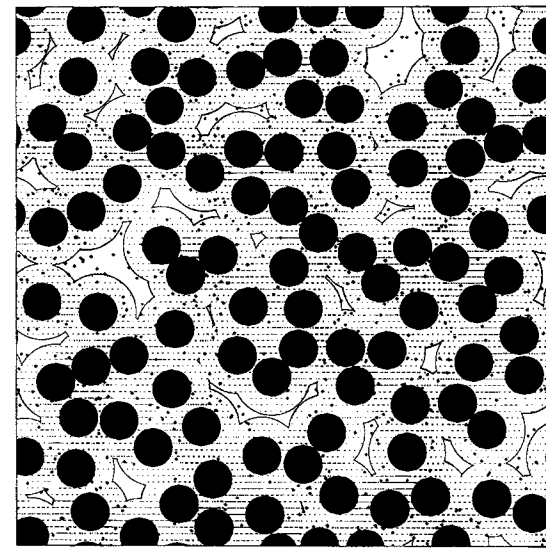

Figure 1. Configuration generated by an RSA process on a random site surface.

Adsorbed solutes and adsorption sites are shown as black circles and points, respectively. Sites which lie within white (unshaded) area are still available for adsorption. The surface coverage of the adsorbed solutes is $\theta = 0.3819$.

Recently, the RSA method has been extended to the random site surface (RSS), which provides a model for affinity adsorbents (Jin et al., 1993). In this model, the adsorption sites are represented as points which are randomly distributed on the surface. The justification for this is that an affinity adsorbent, in general, is produced by immobilizing certain affinity ligands on porous silica, agarose, and synthetic polymers. Although the active ligands may be regularly spaced on a one-dimensional polymer chain, the random folding of these chains during the formation of the adsorbent particle results in a disordered distribution of the active groups on the adsorbent surface. Due to their finite size, the distribution of the ligands cannot be completely random, however, we believe that the RSS provides a reasonable description.

As indicated, RSA is a model for irreversible adsorption. However, most systems which are important for separation or catalysis involve reversible adsorption. Generalized RSA processes, which permit either desorption or surface diffusion, have been introduced by Tarjus et al. (1990). The range of validity of the theoretical expansions obtained by these authors is limited to low surface coverages. In this study, we have developed algorithms to simulate RSA with desorption, referred here as random reversible adsorption (RRA), on continuous and random site surfaces. Based on the simulation results, correlations for ϕ as a function of θ on a CS and as a function of θ and ρ_{site} on a RSS are proposed. Subsequently, adsorption equations which properly incorporate the steric hindrance effects

of the preadsorbed solutes on the adsorption kinetics and equilibrium are developed. The equations are then applied to correlate chromatography protein breakthrough curves and adsorption isotherm data for gas adsorption on activated carbon. For the selected systems, the new equations correlate the experimental data much more accurately than the Langmuir equation.

Theoretical Framework and Computer Simulation Algorithms

An important parameter which characterizes the adsorption of spherical particles of diameter σ on a RSS is the relative site density:

$$\alpha = \frac{\pi\sigma^2}{4}\rho_{\text{site}} \tag{3}$$

Physically, α represents the average number of sites contained within an area equal to one solute cross section.

The available surface function on a CS is defined as:

$$\phi = \frac{\text{available surface area}}{\text{total surface area}} \tag{4}$$

while on a RSS, we interpret ϕ as the fraction of sites which are available:

$$\phi = \frac{\text{number of available sites}}{\text{total number of adsorption site of the surface}}. \tag{5}$$

For irreversible adsorption on a CS (denoted as RSA-CS), ϕ is a function only of surface coverage, θ, while for irreversible adsorption on a RSS (denoted as RSA-RSS), ϕ is a function of θ and α.

As first pointed out by Widom (1966), the configurations resulting from an irreversible process (RSA) are different from their equilibrium counterparts. Figure 2 shows an equilibrium adsorption configuration. Although the surface coverage of the configuration is exactly the same as the irreversible configuration shown in Figure 1, the white area (or the number of sites contained within this area) in Figure 2 is larger than that in Figure 1. In other words, at the same surface coverage, an equilibrium configuration has a larger available surface than a configuration generated by an irreversible process. Some insight into this difference is provided by considering a jammed RSA configuration for which the available surface is zero. The equilibrium system at the same coverage is characterized by fluctuations which ensure that the available surface is nonzero. RSA is a highly inefficient way to cover a surface. Any relaxation mechanism allows for more efficient packing and leads eventually to equilibrium.

For random reversible adsorption on a CS (denoted as RRA-CS), ϕ is a function of both θ and K^*:

$$\phi = \phi(\theta, K^*) \tag{6}$$

where K^* is defined as:

$$K^* \equiv \frac{k_a c}{k_d} \tag{7}$$

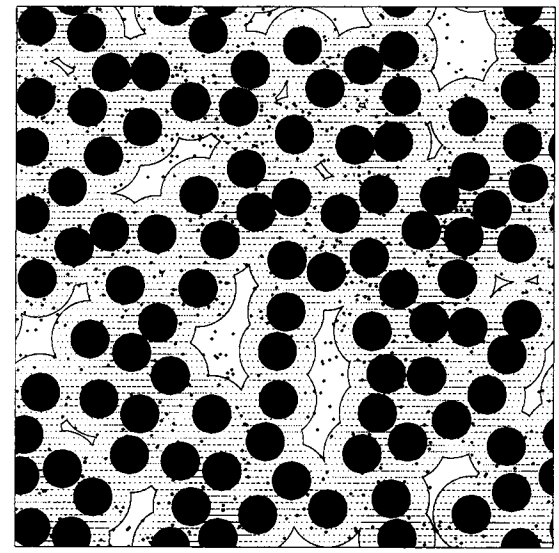

Figure 2. Same as Figure 1, except that the configuration is an equilibrium one.

Note that although coverage is the same as in Figure 1, the available surface (white area) is larger.

At equilibrium, the surface coverage, θ^{eq}, becomes a unique function of K^*. Therefore:

$$\phi^{eq} = \phi^{eq}(\theta^{eq}) \tag{8}$$

Similarly, for random reversible adsorption on a RSS (denoted as RRA-RSS), ϕ is a function of θ, K^* and α:

$$\phi = \phi(\theta, K^*, \alpha) \tag{9}$$

while at equilibrium, ϕ^{eq} is described by:

$$\phi^{eq} = \phi^{eq}(\theta^{eq}, \alpha) \tag{10}$$

Various theories for $\phi^{RSA}(\theta)$ (Schaaf and Talbot, 1989a), and $\phi^{RSA}(\alpha,\theta)$ (Jin et al., 1993) have been tested with simulations. In this work, we extend the simulation methodology to include desorption. For irreversible adsorption on a CS, the computer simulation process can be summarized as follows. Starting from a clean surface, a position on the surface is randomly chosen. If a solute, when centered in this location, does not overlap with any of preadsorbed solutes on the surface, the adsorption attempt is accepted and the solute remains at the position permanently; otherwise the particle is removed. The surface coverage, θ, and ϕ^{RSA} are evaluated periodically. Attempts are made to add new particles until the system is close to saturation. The final jamming limit configuration is reached by randomly placing solutes in the tiny target areas present, and the jamming limit surface coverage, θ_∞, is evaluated. All the simulations were performed in a square area ($L \times L$) with periodic boundaries. The system size is characterized by the relative area of one solute:

$$a = \frac{\pi\sigma^2}{4L^2} \tag{11}$$

The smallest time unit in the simulation is the interval between two sequential adsorption attempts. With this time unit, θ depends not only on the number of adsorption attempts, N_a, but also on the system dimension used for the simulation. For example, after the first adsorption attempt, the coverage is $\theta(N_a=1)=\pi\sigma^2/4L^2$, where σ is the solute diameter. We therefore define a reduced simulation time, t^*, as:

$$t^*=\frac{\pi\sigma^2}{4L^2}N_a \tag{12}$$

so that $\theta(t^*)$ is independent of system dimension.

For the RSA-RSS process, the simulation is similar to that described above except that initially N_{site} adsorption sites are placed randomly in the square of area L^2. For each adsorption attempt, a trial solute is centered on a site selected at random. If there is no overlap, the solute remains on the site permanently, otherwise the solute is rejected. The evaluation of $\phi^{RSA}(\alpha,\theta)$ and the jamming limit coverage, $\theta_\infty(\alpha)$, in this case, is much simpler than for the RSA-CS process since the available sites can be easily identified. The simplest way to reach the jamming configuration in the final stage is to loop through the available sites in the same order in which they were generated. In this way the jamming configuration can be reached in just N_{site} attempts.

The relationship between t^* and the time, t, appearing in Eq. 2 may be established by considering the first simulation step ($N_a=1$) during which one particle is placed on an empty surface. According to Eq. 2, the time interval, Δt, for this event is:

$$\Delta t=\frac{\pi\sigma^2}{4L^2k_ac} \tag{13}$$

Comparison with Eq. 12 shows that:

$$t^*=k_ac t \tag{14}$$

For reversible adsorption, the algorithm is the same as described above, except that after each simulation step, all adsorbed solutes desorb with probability P_{des}. Therefore, in one simulation time step, Δt, the average number of particles desorbed, $-\Delta N$, is NP_{des}, where N is the total number of particles on the surface. However, ΔN can also be expressed as:

$$\Delta N=-k_dN\Delta t \tag{15}$$

Using the value of Δt (Eq. 13) we establish the relationship connecting P_{des}, k_ac, k_d and system dimension:

$$P_{des}=\frac{\pi\sigma^2}{4L^2k_ac}k_d \tag{16}$$

To test a particular solute for desorption a uniform random number, ζ ($0<\zeta<1$), is generated by the computer: if $\zeta<P_{des}$, then the solute is removed from the surface; otherwise it stays. Such adsorption-desorption processes continue until equilibrium is reached at which $\phi^{eq}=(4L^2/\pi\sigma^2)\,P_{des}\theta^{eq}$.

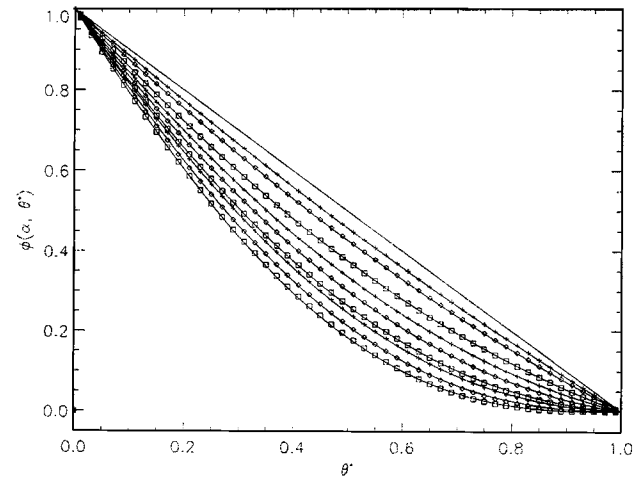

Figure 3. Available surface function, ϕ, as function of normalized surface coverage, θ^*, for the RSA-RSS process.

From top to bottom: $\alpha=0$ (Langmuir), 0.1, 0.2, 0.5, 1.0, 2.0, 5.0, 9.0, 50, and ∞ (continuous surface). Points are computer simulation data and solid lines are predictions of Eq. 23 for finite values of α and Eq. 22 for the continuous surface ($\alpha=\infty$).

Simulation Results and Correlations

In adsorption experiments, the accessible quantity is usually the amount adsorbed per unit mass or per unit volume of the adsorbent, here denoted by q. Only if the specific surface area of the adsorbent and the exact molecular dimensions of the solute are known, is it possible to compute the absolute surface coverage, θ. For the purpose of comparing with experiment, the relevant quantity is the normalized surface coverage:

$$\theta^*=\frac{\theta}{\theta_\infty} \tag{17}$$

since for monolayer adsorption θ^* is equivalent to the ratio of q to the maximum adsorption capacity, q_m. Figure 3 displays $\phi^{RSA}(\alpha,\theta^*)$ vs. θ^*.

Schaaf and Talbot (1989a) found an analytic expansion of ϕ^{RSA} on a CS as a function of θ, which is accurate in the coverage range, $0\le\theta<0.25$:

$$\phi^{RSA}=1-4\theta+\frac{6\sqrt{3}}{\pi}\theta^2+1.4069\theta^3+0(\theta^4) \tag{18}$$

According to Pomeau (1980) and Swendsen (1981), the coverage evolves as a power law near the jamming limit:

$$(\theta_\infty-\theta)\sim\xi t^{*-1/2} \tag{19}$$

where ξ is a constant which we estimate as 0.2455 from our simulation results. Since ϕ^{RSA} is related to θ as:

$$\frac{d\theta}{dt^*}=\phi^{RSA}(\theta) \tag{20}$$

then near the jamming limit coverage:

$$\phi^{RSA}(\theta)=\frac{1}{2\xi^2}(\theta_\infty-\theta)^3$$

$$(\text{or } \phi^{RSA}(\theta^*)=\frac{\theta_\infty^3}{2\xi^2}(1-\theta^*)^3=\xi^o(1-\theta^*)^3) \quad (21)$$

For $\xi=0.2455$ and $\theta_\infty=0.5474$, ξ^o is 1.355.

Based on the known behavior of ϕ^{RSA}, the following semi-empirical equation is proposed:

$$\phi^{RSA}(\theta^*)=\frac{(1-\theta^*)^3}{1+a_1\theta^*+a_2\theta^{*2}+a_3\theta^{*3}+a_4\theta^{*4}} \quad (22)$$

where $a_1=-0.8120$, $a_2=0.2366$, $a_3=0.0845$, and $a_4=0.2330$. The coefficients and the form of the equation have been chosen to reproduce both the short-time (Eq. 18) and asymptotic (Eq. 21) behavior. Equation 22 describes the simulation results more accurately than the previous fitting functions proposed by Schaaf and Talbot (1989b).

The fit to the simulation data may be further improved by allowing all the coefficients in Eq. 22 to vary freely, with the result that $a_1=-0.8237$, $a_2=0.4580$, $a_3=-0.6700$, and $a_4=0.8700$. As can be seen in Figure 3 (the lowest curve, $\alpha=\infty$), the agreement between this fitting function and simulation data is excellent.

An analytic solution of $\phi^{RSA}(\theta^*,\alpha)$ has been found by Jin et al. (1993) based on a mapping between the RSA-RSS and RSA-CS processes. However, the solution is quite complicated for practical purposes. We therefore developed a simple empirical equation of $\phi^{RSA}(\theta^*;\alpha)$ which is accurate over the entire θ^* and α ranges:

$$\phi^{RSA}(\theta^*;\alpha)=(1-\theta^*)(1-B_1\theta^*-B_2\theta^{*2})^2 \quad (23)$$

where B_1 and B_2 are functions of α:

$$B_1=\frac{0.7126\alpha+1.404\alpha^{1.5}}{1+3.4363\alpha+2.4653\alpha^{1.5}} \quad (24)$$

$$B_2=\frac{0.07362\alpha+0.1204\alpha^{1.5}}{1+0.5443\alpha+0.2725\alpha^{1.5}} \quad (25)$$

We note that the form of Eq. 23 has the desired properties of $\phi^{RSA}(\theta^*=0,\alpha)=1$, $\phi^{RSA}(\theta^*=1,\alpha)=0$, and $\phi^{RSA}(\theta^*,\alpha=0)=1-\theta^*$). Comparisons between the simulation data and Eq. 23 (the solid lines) are shown in Figure 3.

For the RSA-RSS process, the simulated values of $\theta_\infty(\alpha)$ at different α values are plotted as points in Figure 4. At least 40 runs are made for each α, and the data shown in Figure 4 are the average values. The relation between $\theta_\infty(\alpha)$ and α can be very well represented by the following equation (Jin et al., 1993):

$$\theta_\infty(\alpha)=0.547\left(1-\frac{1+0.3136\alpha^2+0.45\alpha^3}{1+1.8285\alpha+0.5075\alpha^3+\alpha^{7/2}}\right) \quad (26)$$

shown as solid line in Figure 4.

Similarly, for the RSA-RSS process, the normalized surface coverage, $\theta^*(t^*,\alpha)$, is defined as:

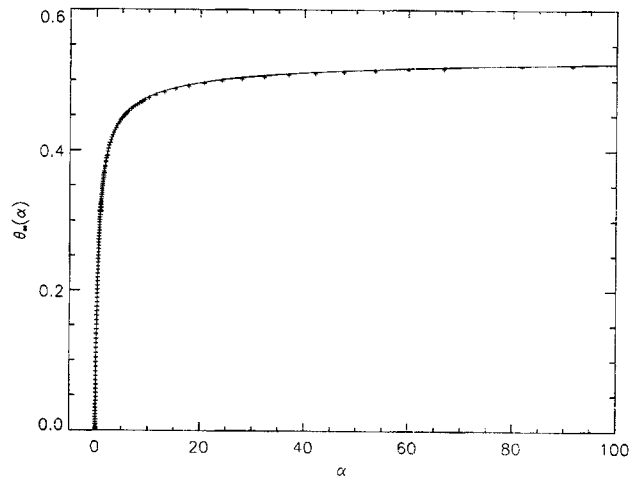

Figure 4. Saturation coverage, $\theta_\infty(\alpha)$, as function of relative site density, α, for RSA-RSS process.

Simulation results are shown as crosses, and solid line shows predictions of Eq. 26.

$$\theta^*(t^*;\alpha)=\frac{\theta(t^*;\alpha)}{\theta_\infty(\alpha)} \quad (27)$$

A number of selected simulation results for $\phi^{RSA}(\theta^*,\alpha)$ vs. θ^* at a fixed α are plotted in Figure 3.

We next consider reversible adsorption processes. $\phi^{RRA}(\theta,K^*)$ from computer simulation at four different values of K^* are plotted in Figure 5 together with ϕ^{RSA} and ϕ^{eq} in a narrow coverage range near equilibrium. At the same surface coverage, ϕ^{eq} is always greater than ϕ^{RSA}. However at low coverages, ϕ^{RSA} and ϕ^{eq} appear to be very close to each other. For a given ϕ, the corresponding equilibrium coverage is always higher than that of irreversible adsorption. The kinetic history of reversible adsorption always lies between the irreversible ad-

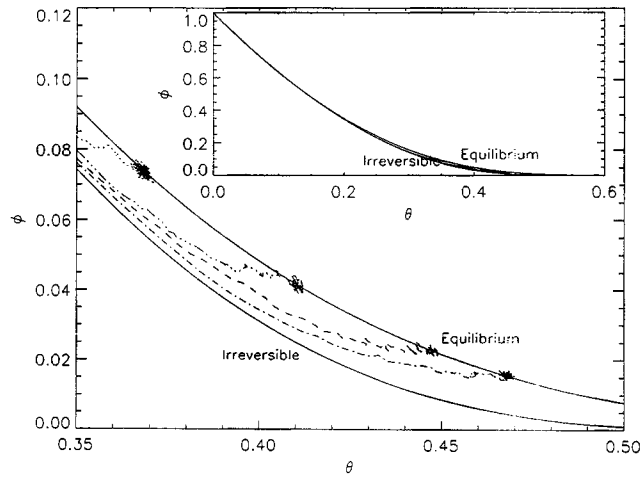

Figure 5. Adsorption kinetics on continuous surface.

The bottom line shows irreversible, or RSA kinetics, while broken lines show four examples of transient kinetics with $K^*=5$, 10.0, 20.0, and 30 (top to bottom). The upper line is locus of equilibrium states that transient curves approach. Inset shows behavior over entire coverage range.

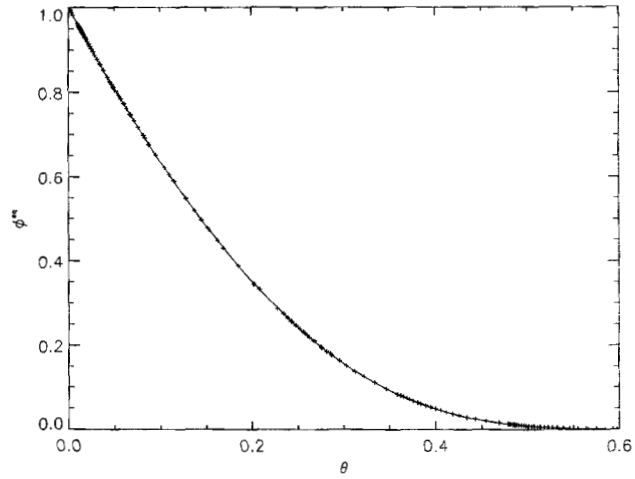

Figure 6. $\phi^{eq}(\theta)$ vs. θ on continuous surface: simulation data (+) and prediction of Eq. 28 (—).

sorption line and the equilibrium curve (see Figure 5), that is, $\phi^{RSA}(\theta) \le \phi^{RRA}(\theta,K^*) \le \phi^{eq}(\theta)$. The reason for this has already been hinted at: the dynamic rearrangement of configuration which accompanies desorption frees additional available surface. At a given coverage in a disordered system, the available surface is a maximum at equilibrium. It is worth noticing that near equilibrium, $\phi^{RRA}(\theta,K^*)$ decreases very slowly.

Schaaf and Talbot (1989b) presented an equation for ϕ^{eq} as a function of θ, which is derived from a semi-empirical equation of state proposed by Henderson (1975):

$$\phi^{eq} = \exp\left(2 - \frac{2}{(1-\theta)^2} + \frac{7}{8}\frac{\theta}{(1-\theta)^2} + \frac{7}{8}\ln(1-\theta)\right) \qquad (28)$$

Comparison with simulation data (Figure 6) shows that this equation is accurate at least for the range of coverage studied in our simulation, $0 \le \theta \le 0.60$. It is known that the accuracy decreases as the coverage increases. One problem with Eq. 28 is that ϕ^{eq} approaches zero at $\theta = 1$, which is physically inconsistent since the maximum possible monolayer coverage is 0.9069, that is, the coverage that corresponds to close triangular packing (Berryman, 1983).

For RRA-RSS process, as indicated by Eqs. 9 and 10, ϕ is a function of three independent variables for kinetics and two independent variables at equilibrium. Here we report the simulation results for $\phi^{eq}(\theta,\alpha)$ vs. θ at different α (see Figure 7) and $\phi^{RRA}(\theta,\alpha=6,K^*)$ vs. θ for various values of K^* (see Figure 8). We see that at a fixed α, similar to the RRA-CS process, $\phi^{RRA}(\alpha,\theta,K^*)$ always lies between $\phi^{RSA}(\alpha)$ and the $\phi^{eq}(\alpha,\theta^{eq})$.

Tarjus et al. (1990) have obtained the coverage expansion for $\phi^{RRA}(\theta,K^*)$ to third order. However, only values of $K^* \le 2$ are within the range of validity of the expansion. At present, no theories or empirical correlation equations are available for the $\phi^{RRA}(\alpha,\theta,K^*)$ and $\phi^{eq}(\alpha,\theta^{eq})$. However, from the simulation results, we conclude the following:

(1) For adsorption on a CS, a system with a small K^* has a low equilibrium coverage, θ^{eq}, and $\phi^{RRA}(\theta,K^*)$ is almost identical to $\phi^{RSA}(\theta)$ in the range $0 \le \theta \le \theta^{eq}$. Therefore, $\phi^{RRA}(\theta,K^*)$ can be well approximated by $\phi^{RSA}(\theta)$.

(2) For a system with a very large K^* the adsorption process is effectively irreversible over a relatively long time interval which may be comparable to the time scale of experiment; therefore the adsorption kinetics can still be well represented by that of irreversible adsorption. The reversible kinetics becomes quite different from that of irreversible adsorption at the later stages.

(3) For adsorption on a RSS, at a given K^*, the higher the α, the greater the difference between $\phi^{RSA}(\alpha,\theta)$ and $\phi^{RRA}(\alpha,\theta,K^*)$. The largest difference between them occurs at $\alpha \to \infty$ which is the case for adsorption on a CS. Therefore, conclusions 1 and 2 apply, a fortiori, for adsorption on a RSS.

Based on the observations listed above we propose that ϕ^{RSA} or ϕ^{eq} be used to represent the reversible adsorption kinetics on a CS at low-to-intermediate coverage, that is,

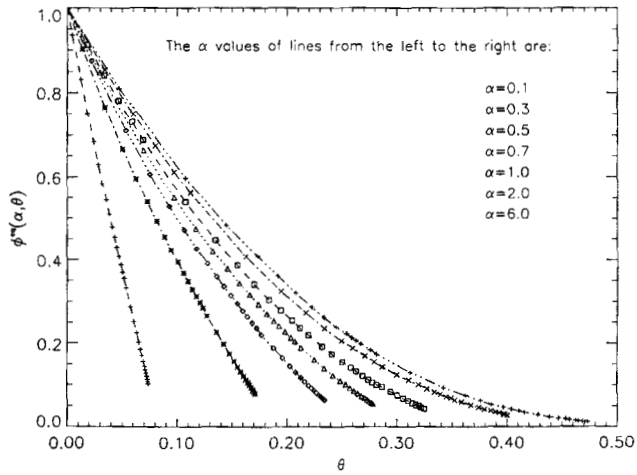

Figure 7. Simulation results of $\phi^{eq}(\alpha,\theta)$ vs. θ on random site surface.

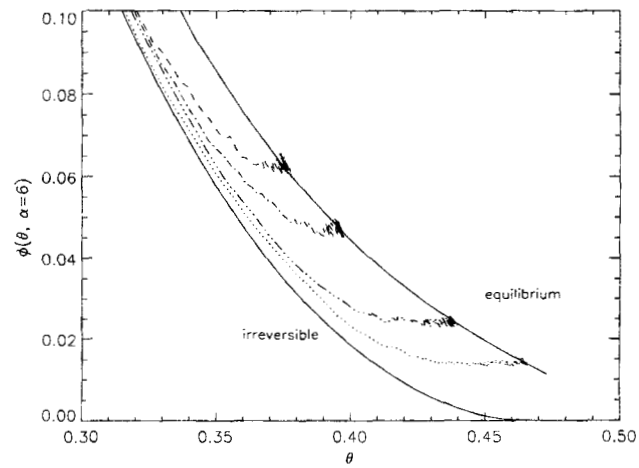

Figure 8. Adsorption kinetics on random site surface at $\alpha = 6$.

The bottom line shows irreversible kinetics, while broken lines show four examples of transient kinetics with $K^* = 6.0$, 8.4, 18.0, and 33.5 (top to bottom). The upper line is the locus of equilibrium states that transient curves approach.

$$\frac{d\theta^*}{dt} = k_a c \frac{(1-\theta^*)^3}{1-0.8237\theta^* + 0.4580\theta^{*2} - 0.6700\theta^{*3} + 0.8700\theta^{*4}} - k_d\theta^* \tag{29}$$

or

$$\frac{d\theta^*}{dt} = k_a c \exp\left(2 - \frac{2}{(1-\theta^*)^2} + \frac{7}{8}\frac{\theta^*}{(1-\theta^*)^2} + \frac{7}{8}\ln(1-\theta^*)\right) - k_d\theta^* \tag{30}$$

For adsorption on a RSS, since only ϕ^{RSA} is known, the approximate kinetic equation proposed is:

$$\frac{d\theta^*}{dt} = k_a c(1-\theta^*)(1 - B_1(\alpha)\theta^* - B_2(\alpha)\theta^{*2})^2 - k_d\theta^* \tag{31}$$

where θ^* is defined in Eq. 27 and the coefficients B_1 and B_2 are given by Eqs. 24 and 25, respectively.

The corresponding adsorption isotherms can be obtained from Eqs. 29, 30, and 31 by setting $d\theta^*/dt = 0$. Obviously, for adsorption on a CS, better results are expected with Eq. 30 which is derived from an (equilibrium) equation of state. As mentioned before, for practical applications, the value of θ^* in the equations can be substituted by q/q_m.

We note that the jamming limit coverage (or the absorption capacity) is a function of α as given by Eq. 26. Therefore, Eqs. 29 and 30, as well as Eq. 31 have the same number of parameters (q_m, k_a, and k_d) as the Langmuir kinetic equation.

We note that the difference between actual adsorption kinetics and the one represented by Eq. 29 or 31 can be further minimized by using an apparent $\theta_\infty(q_m)$, k_a, or k_d in the correlation. For example, in Figure 9, by the simulation, the actual adsorption kinetics [$\theta(K^*,t^*)$ vs. t^*] for $K^* = 7.875$ on a CS is represented by the points. The kinetics calculated by Eq. 29 with the same value of K^* and with $\theta_\infty = 0.547$ which corresponds to the irreversible jamming limit surface coverage, are plotted as the dashed line. Obviously, the dashed line is below the actual adsorption kinetics since ϕ^{RSA} is smaller than ϕ^{RRA}. However, if we use the same K^* but let $\theta_\infty = 0.582$, the calculated kinetics, as indicated by the dotted line in Figure 9, becomes quite close to the actual adsorption kinetics. A still more accurate correlation, as represented by the solid line in Figure 9, is obtained by using a set of apparent parameters: $K^* = 16.136$ and $\theta_\infty = 0.537$.

To illustrate the difference and similarity between the Langmuir equation and the equations proposed here, we define an apparent adsorption rate constant, k_a^*:

$$k_a^* = k_a\left(1 - \frac{0.7126\alpha + 1.404\alpha^{1.5}}{1 + 3.4363\alpha + 2.4653\alpha^{1.5}}\theta^* - \frac{0.07362\alpha + 0.1204\alpha^{1.5}}{1 + 0.5443\alpha + 0.2725\alpha^{1.5}}\theta^{*2}\right)^2 \tag{32}$$

then Eq. 31 may be rewritten as:

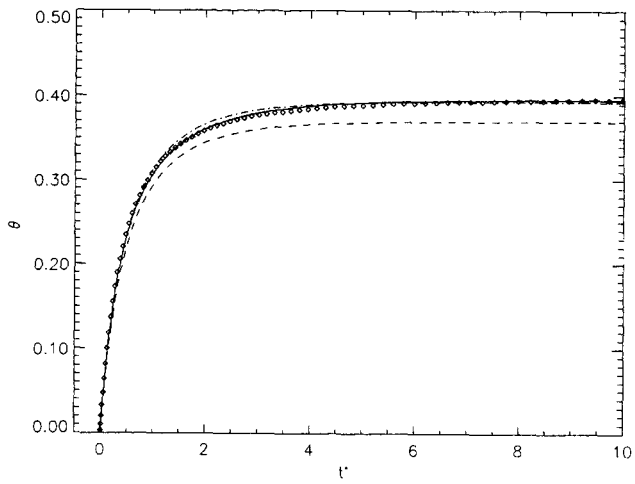

Figure 9. Surface coverage, θ, vs. simulation time, t^*, for reversible adsorption on continuous surface.

Diamonds show simulation results with $K^* = 7.875$. Lines were computed by Eq. 29 with: $K^* = 7.875$ and $\theta_\infty = 0.547$ (----); $K^* = 7.875$ and $\theta_\infty = 0.582$ (••••); and $K^* = 16.136$ and $\theta_\infty = 0.537$ (——).

$$\frac{d\theta^*}{dt} = k_a^* c(1-\theta^*) - k_d\theta^* \tag{33}$$

which has the same form as the Langmuir equation except that k_a^* is a function of α and θ^*. At a very small (or zero) α or at low coverage, k_a^* is almost equal to k_a and Eq. 31 reduces to the Langmuir equation. However as α or θ^* increases, the difference between the two equations becomes significant.

Experimental Data Correlation and Discussions

In this section, we use experimental data to test the validity of the kinetic or isotherm equations developed here. As mentioned before, the random site surface (RSS) is a model for an affinity adsorbent, while the continuous surface (CS) is appropriate for systems with hydrophobic interactions. We have applied the equations to correlate protein breakthrough curves on an affinity chromatography column (a kinetic process) and isotherms of ethane and ethylene adsorption on activated carbon and a molecular sieve, respectively. In the former, large solutes in an aqueous solution adsorb on a random site surface, while the other systems have small molecules in a gaseous state, which adsorb on a continuous surface.

Correlation of breakthrough curves of a protein

To test the validity of Eq. 31 for an affinity adsorption system, it has been incorporated into the VERSE-LC (VErsatile Reaction-SEparation model for liquid chromatography) computer program (Berninger et al., 1991) in place of the Langmuir kinetic equation. This new version of the VERSE-LC program was used to correlate the data of Mao et al. (1991) who reported lysozyme breakthrough curves on a chromatography column packed with 1.5 μm diameter nonporous silica beads with Cibacron Blue F3GA immobilized on the surface. The principal reason for selecting this data is that the adsorbent is nonporous,

so that intraparticle diffusion is absent and the intrinsic adsorption kinetics is expected to be the rate controlling step. In order to calculate the breakthrough curves of this system using VERSE, the values of k_a and k_d, α, q_m, and film mass-transfer coefficient, K_f, are needed. For the latter, we used the same value reported by Mao et al. (1991), that is, $K_f = 3.4 \times 10^{-4}$ (m/s). If the site density and solute size were known, α could be calculated by Eq. 3. However, Mao et al. did not report the site density of Cibacron Blue F3GA on the nonporous silica beads, mentioning only that it was high. Therefore α, together with the values of k_a, k_d, and q_m, were determined by the best fit of the experimental data.

Mao et al. themselves had tried to correlate the experimental data by using the Langmuir kinetic equation. The experimental data and the effluent histories correlated by the Langmuir equation (from Mao et al.) and by our equation with $\alpha = 9$ are plotted in Figure 10 as indicated by the symbols, the dashed lines, and the solid lines, respectively. The corresponding simulation parameters used to fit the breakthrough curves by the two equations are listed in Table 1.

From Figure 10, we can see that the Langmuir equation fits the initial part of the experimental breakthrough curves but fails to predict the slow approach to saturation. However, these curves are fitted very precisely with the new adsorption kinetic Eq. 31. Furthermore, the fit of the data by the Langmuir kinetic equation requires a different set of k_a and k_d for each breakthrough curve at a different solute concentration, c_o, whereas the new kinetic equation is able to fit all the breakthrough curves at the five different values of c_o, using just one set of k_a and k_d (see Table 1).

According to our simulation results, $\theta_\infty(\alpha = 9)$ is about 0.47. For a nonporous adsorbent, the experimental θ_∞ can be estimated from the information of q_m, solute diameter, and column packing. According to Table 1, the average q_m for this system is about 4.57 [mg(lysozyme)/mL(adsorbent)]. The molecular dimensions of lysozyme are reported as $45 \times 30 \times 30$ Å(Jolles and Jolles, 1984). If we take the effective lysozyme diameter as 35 Å, then we estimate the experimental θ_∞ as 0.4665. This is surprisingly close to that obtained from simulation. The result in one way supports our argument that with a large K^* the adsorption is effectively irreversible on the time scale of the experiment. On the other hand, it gives a justification for the proposed value of α.

For both the Langmuir equation and the new kinetic equation, q_m must be varied in order to match the lysozyme breakthrough times at different concentrations. In our case, q_m consistently increases with lysozyme concentration in the solution. However, in the result reported by Mao et al., q_m varied randomly. The consistent increase of q_m with c may result from one or more of the following: (1) loss or degradation (or fouling) of immobilized Cibacron Blue ligands during experiments (if high concentration runs preceded the low concentration runs); (2) aggregation of lysozyme; and (3) more than one adsorption orientation for lysozyme on the solid surface.

Aggregation of proteins in solution and on solid surfaces has been reported previously (Kunitan et al., 1988; Karger and Blanco, 1989; Grinberg et al., 1989; Blanco et al., 1989). In a system with solute aggregation, the fraction of aggregates to monomer is higher at a higher c, which in turn gives a higher fraction of aggregates to monomer on the solid surface. The surface area occupied by an aggregate of n monomers is, in general, less than the sum of areas occupied by n monomers independently. Therefore, on the same surface area the total amount of solutes (in terms of monomers) adsorbed, and hence q_m, increases with increasing c.

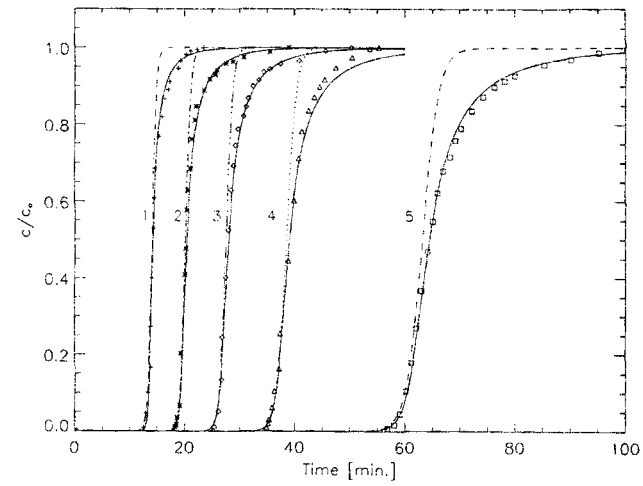

Figure 10. Prediction of Lysozyme breakthrough curves by LE (----) and by Eq. 31 (—).

Symbols are experimental data of Mao et al. (1991). Bulk concentrations, c_o, corresponding to each of five breakthrough curves, together with model parameters, are listed in Table 1.

A possible explanation for the effect of orientation is as follows. Since k_d is very small the adsorption process may be considered as irreversible on the limited experimental time scale. Lysozyme may adsorb with two different orientations, with either the side of 45 Å × 30 Å, defined as "side-on," or with the side of 30 Å × 30 Å defined as "end-on." We assume that molecules in an "end on" orientation have a tendency to convert (irreversibly) to "side on" since in the latter state, the molecule contacts a larger area of the solid surface and is thermodynamically more stable. The initial ratio of the two orientations may be considered to be independent of c. However, more solutes with initial "end-on" orientations can convert to "side-on" orientations at low bulk concentration. In this case, total adsorption rate is slow, and new solutes are less likely to arrive in the neighborhood of an adsorbed solute before it has the time to complete its orientational conversion. As a result, the lower the c, the greater the fraction of solutes with the "side-on" orientation and hence the smaller the q_m. Orientation effects were reported experimentally by Brynda et al. (1986) and explained by Lundstrom (1983).

Table 1. Simulation Parameters Used to Predict Breakthrough Curves of Lysozyme by LE and Eq. 31 at $\alpha = 9$*

Curve No.	c_o, (mg/mL)	q_m, (mg/mL Sorbent)		k_a, (mL/mg·min)		k_d, (1/min)	
		LE	EQ31	LE	EQ31	LE	EQ31
1	0.100	5.030	5.050	26.88	40.00	0.1478	0.002
2	0.065	4.825	4.750	33.90	40.00	0.1865	0.002
3	0.045	4.722	4.532	38.88	40.00	0.2138	0.002
4	0.030	4.671	4.425	36.30	40.00	0.1997	0.002
5	0.018	5.082	4.425	38.88	40.00	0.2138	0.002

*The parameters listed under LE are from Mao et al. (1991). The predicted breakthrough curves are plotted in Figure 10 with the corresponding curve number indicated.

Table 2. Correlation Results for System of Ethane Adsorption on Activated Carbon at Four Different Temperatures*

Equation	T(K)	q_m	K	Root MSE	R-Square
Langmuir	293.15	5.7801	0.010434	14.40930	0.9929
Eq. 29	293.15	7.8921	0.013377	4.90013	0.9992
Eq. 30	293.15	13.3570	0.009030	3.60271	0.9996
Langmuir	313.15	5.4425	0.007457	14.04839	0.9945
Eq. 29	313.15	7.7740	0.007869	4.66447	0.9994
Eq. 30	313.15	13.3681	0.004969	3.08406	0.9997
Langmuir	333.15	5.0454	0.005156	11.51479	0.9963
Eq. 29	333.15	7.6358	0.004457	4.96860	0.9993
Eq. 30	333.15	13.3543	0.002587	3.98463	0.9995
Langmuir	363.15	4.4535	0.003580	9.32515	0.9974
Eq. 29	363.15	7.2182	0.002581	5.02423	0.9993
Eq. 30	363.15	12.8174	0.001480	4.50993	0.9994

*From Szepesy and Illes (1963).

Correlation of adsorption isotherm data

In this section, the two parameter (q_m and K) isotherm forms of Eqs. 29 and 30 are used to correlate the isotherm data of ethane adsorption on activated carbon at 293.15, 313.15, 333.15, and 363.15 K (Szepesy and Illes, 1963). Ethane adsorption on activated carbon is a physical adsorption process, which suggests that the carbon surface can be considered as continuous and Eqs. 29 and 30 can be used. For comparative purposes, the isotherm data are also correlated by the Langmuir equation. The correlations are performed with the SYNLIN procedure from the SAS computer software (Cary, 1988). The best fitting parameters (q_m and K), together with the root mean square error (Root MSE) and R-square value (R-square = 1 for perfect fit) of the correlation for the three equations at different temperatures, T, are listed in Table 2. Comparison between the experimental data and the correlations by Eq. 30 are shown in Figure 11. We observe that: (1) according to the Root MSE or R-square values, the two equations which incorporate the steric hindrance effect fit the experimental data more accurately than the Langmuir equation at all temperatures; (2) between Eqs. 30 and 29, slightly better correlations are obtained with Eq. 30; (3) q_m from Eq. 30 is about twice of that from Eq. 29; (4) the values of K obtained from all three equations decrease as the temperature increases; and (5) q_m by Eq. 29 and the Langmuir equation vary with temperatures, with variations of about 9.0% and 26%, respectively. However, with Eq. 30 an almost identical q_m is obtained except at 333.15 K.

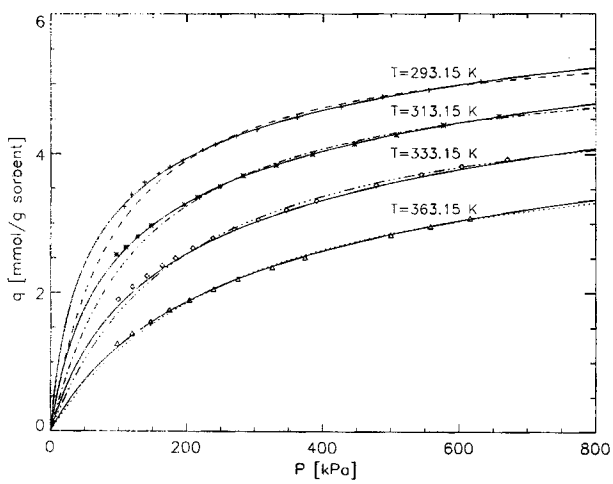

Figure 11. Correlation of isotherm data for adsorption of ethane on activated carbon by LE (----) and Eq. 30 (—).

Symbols show experimental data of Szepesy and Illes (1963).

Result 1 shows that adsorption models which account for the steric hindrance effects can represent the experimental data much better than the Langmuir equation. Result 2 is anticipated because Eq. 30 uses ϕ^{eq}, while Eq. 29 approximates ϕ^{eq} with ϕ^{RSA}. For result 3, the large difference between q_m from Eqs. 29 and 30 can be explained by the different jamming limit coverage values used in the two equations, that is, 0.5474 and 1.0, respectively. The equilibrium constant, K, is inversely proportional to q_m. The decrease of K with increasing temperature as mentioned in 4 above is thermodynamically consistent for an exothermic adsorption process. Probably, the most significant result is observation 5; that is, q_m obtained from Eq. 30 at various temperatures is nearly constant. By definition, q_m is the amount adsorbed on the surface as solute concentration approaches infinity. With this definition, q_m is a purely geometric property if the solute contains a hard core. Therefore, q_m should be independent of temperature provided that the thermal expansion of the adsorption surface and solute size is negligible. This near invariance of q_m with temperatures is another strong indicator of the validity and physical significance of the new adsorption equation. For comparison, we note that Valenzuela and Myers (1989) correlated the same sets of data using the Toth (Toth, 1971) and UNILAN (Honig and Reyerson, 1952) equations. Even with these three parameter isotherm equations, q_m is not constant: about a 9% variation for the Toth and 21% for the UNILAN were reported.

Similar correlation results are obtained for the adsorption isotherm data of ethylene adsorption on a molecular sieve at 212.70, 260.20, and 301.40 K (Nakahara et al., 1974). The correlation results and the parameters from the correlations are listed in Table 3.

In practice, one identifies whether an adsorption isotherm is of the Langmuirian type by a Scatchard plot (Scatchard, 1949) of the isotherm data: only if the plot is linear is the isotherm regarded as Langmuirian. The curvature in a Scatchard plot is commonly interpreted as either the result of multisite binding or heterogeneous adsorption sites or both. As

Table 3. Correlation Results for System of Ethylene Adsorption on Carbon Molecular Sieve at Three Different Temperatures*

Equation	T(K)	q_m	K	Root MSE	R-Square
Langmuir	278.65	2.7648	0.1183	2.26087	0.9948
Eq. 29	278.65	3.5419	0.2146	0.27326	0.9999
Eq. 30	278.65	5.8568	0.1640	0.44255	0.9998
Langmuir	303.15	2.5073	0.0745	2.21109	0.9952
Eq. 29	303.15	3.4771	0.0873	1.09213	0.9988
Eq. 30	303.15	5.8810	0.0591	0.95146	0.9990
Langmuir	323.15	2.2416	0.0483	1.75613	0.9969
Eq. 29	323.15	3.3212	0.0444	1.22516	0.9985
Eq. 30	323.15	5.8010	0.0265	1.15294	0.9985

*From Nakahara et al. (1974).

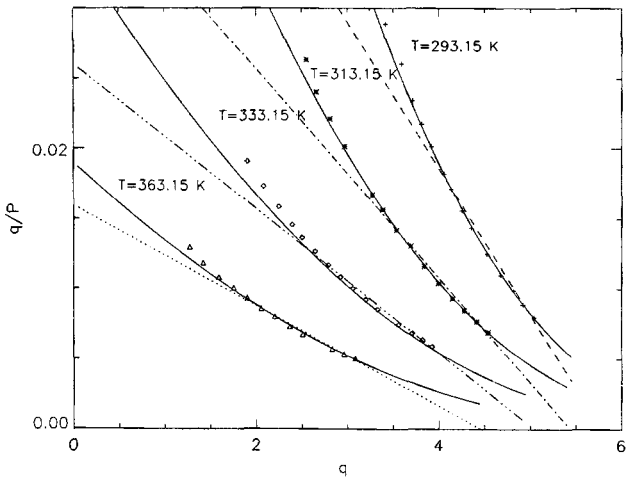

Figure 12. Scatchard plots of experimental data and correlation results in Figure 11.

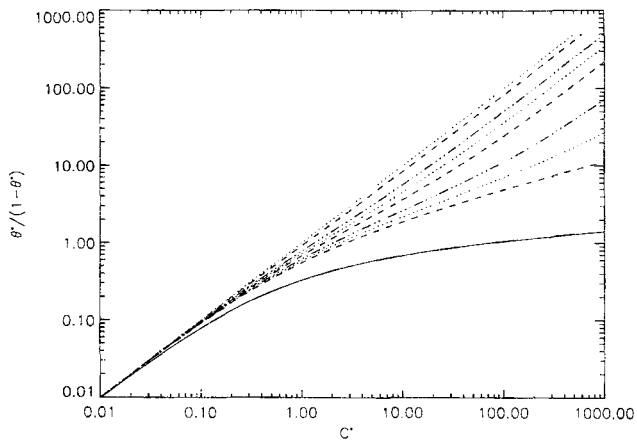

Figure 14. Hill plots of isotherm form of Eq. 31 with $\alpha = 0, 0.1, 0.5, 1.0, 2.0$, and 9.0, 50 and ∞ from top to bottom (----).

Solid line shows isotherm form of Eq. 30.

mentioned in the introduction, if steric hindrance exists, no adsorption (or adsorption isotherm) is Langmuirian. In other words, disregarding other effects, steric hindrance alone can produce curvature in the Scatchard plot. As shown in Figure 12, the previous experimental isotherm data in the form of a Scatchard plot does show curvature which is reasonably represented by the correlations from Eq. 30. Figure 13 shows the general Scatchard plots corresponding to Eq. 31 at different values of α (dashed lines), and Eq. 30 (solid lines).

The Hill plot is also frequently used to identify positive or negative cooperativity in adsorption:

$$\log\left(\frac{\theta}{1-\theta}\right) = \log K + n_H \log c \tag{34}$$

where n_H is the Hill coefficient. For noncooperative adsorption, as with the Langmuir equation, $n_H = 1$. Depending on the value of n_H, an adsorption process is considered to have positive ($1 < n_H$) or negative ($0 < n_H < 1$) cooperativity (Andrade, 1985). Positive cooperativity means that adsorption of previous molecules facilitates adsorption of subsequent molecules, whereas negative cooperativity implies the opposite. From the Hill plots of Eq. 34 at different α values (see Figure 14) we observe that: the larger the value of α and the higher the surface coverage, the smaller the slope (n_H), and all the slopes are less than 1 except at $\alpha = 0$. Therefore, steric hindrance results in a negative cooperativity, which becomes more pronounced as the surface becomes more crowded, or as the relative site density increases.

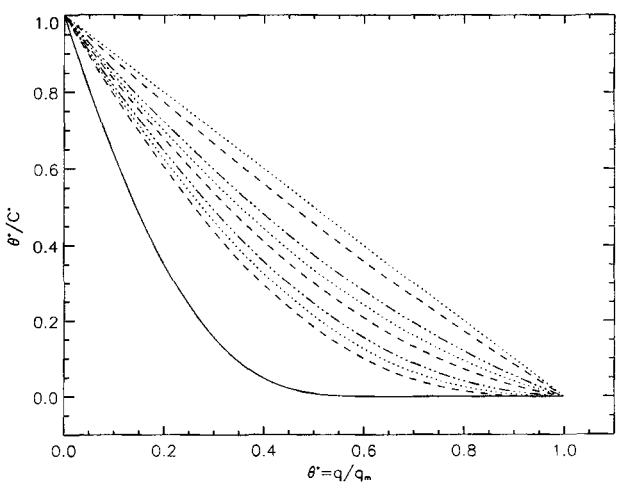

Figure 13. Scatchard plots of isotherm form of Eqs. 31 with $\alpha = 0, 0.1, 0.5, 1.0, 2.0$, and 9.0, 50, and ∞ from top to bottom (----). Solid line shows isotherm form of Eq. 30.

Summary and Conclusions

The term $1-\theta^*$ in the Langmuir equation describes only an ideal adsorption system in which solutes adsorb at isolated sites, which is not the case for most realistic systems. For any system where a solute covers more than one site, the steric hindrance effect must be considered in order to describe the adsorption process accurately. In this work, various models that account for this effect are considered. These kinetic or isotherm models are similar to the Langmuir model except that the term $1-\theta^*$ of the latter is replaced by a general available surface function, ϕ. For irreversible adsorption on a continuous surface (CS), ϕ depends on the surface coverage, while for reversible adsorption kinetics it is also a function of the $K^* = k_a c/k_d$. On a random site surface (RSS), ϕ is a function of the surface coverage and the relative site density, α, for irreversible adsorption, and depends in addition on K^* when the adsorption is reversible. Computer simulation algorithms for evaluating ϕ either for irreversible or reversible adsorption on a CS or on a RSS have been developed. Both kinetic and equilibrium data are obtained from the simulations. The accuracy of various equations proposed for kinetics and isotherms is investigated by comparison with the computer simulation results. The equations are then applied to experimental data correlation. Lysozyme adsorption on an affinity surface has been analyzed using the RSS model, whereas the adsorption of ethane and ethylene on activated carbon and

carbon molecular sieve were analyzed using the CS model. In all cases, good correlation results are obtained. The significance of the models lie not only in their ability to correlate the experimental data more accurately than the Langmuir equation, but also in terms of the physical significance of the adsorption parameters obtained from the correlation; for example, the maximum adsorption capacity (or jamming limit surface coverage).

More specific conclusions are as follows:

(1) At low or intermediate coverage, the Langmuir isotherm equation may fit the experimental data, but the estimated q_m and K are questionable. In general, q_m obtained from the Langmuir equation correlation is lower than the actual maximum adsorption capacity and, as a result, K is overestimated.

(2) Continuous rearrangement of the surface configuration in a reversible adsorption results in a slow approach to equilibrium, and higher ϕ at a fixed θ, and θ_∞ values than those for irreversible adsorption. Therefore, a high affinity adsorption system requires a long time to reach equilibrium.

(3) To correlate adsorption kinetics, Eq. 29 or 31 is recommended, while for isotherm behavior, Eq. 30 gives a better result if the surface can be treated as continuous.

(4) Steric hindrance effects alone result in nonlinear Scatchard and Hill plots with negative cooperativity.

While the adsorption models presented here appear to represent accurately the steric hindrance effects and provide good correlations of the experimental data, some issues remain to be resolved. An accurate equation for the transient adsorption kinetics is still unavailable either on a CS or on a RSS. A more challenging problem is to find the ϕ_i for a multicomponent adsorption system. All these issues are the subjects of our ongoing research.

Acknowledgments

This work was supported by a grant from NSF, EID-9024174 and a fellowship from the Rohm and Haas Company. Dr. R. D. Whitley and Mr. J. A. Berninger incorporated Eq. 31 into the VERSE program, so that the breakthrough curves of lysozyme could be analyzed by our model.

Notation

B_1 = correlation coefficient
B_2 = correlation coefficient
c = solute concentration in solution phase
c_o = initial lysozyme concentration in solution phase
CS = continuous surface
k_a^* = apparent adsorption rate constant
k_a = adsorption rate constant
k_d = desorption rate constant
K = adsorption equilibrium constant (k_a/k_d)
K^* = a constant defined as $k_a c/k_d$
K_f = film mass-transfer coefficient, (m/s)
L = side of cell used in simulation
n_H = Hill plot coefficient
N = number of solutes adsorbed on surface
N_a = number of adsorption attempts
N_{site} = number of adsorption sites on surface
P = gas pressure
P_{des} = desorption probability of a solute in one simulation timestep
q = amount solutes adsorbed in solid surface
q_m = maximum adsorption capacity
RRA = random reversible adsorption
RSA = random sequential adsorption (addition)
RSS = random site surface
t = real adsorption time
t^* = reduced adsorption time in computer simulation
T = temperature

Greek letters

α = relative site density defined in Eq. 3
ΔN = number of solute difference on surface in a time of Δt
Δt = time interval in one simulation step
ζ = value of a random number
θ = surface coverage
θ^* = θ/θ_∞
θ^{eq} = surface coverage at equilibrium
θ_∞ = irreversible jamming limit surface coverage on continuous surface
$\theta_\infty(\alpha)$ = irreversible jamming limit surface coverage on random site surface
ξ = constant coefficient
ξ^o = constant coefficient
ρ_{site} = adsorption site density
σ = solute diameter
ϕ = available surface function
ϕ^{eq} = available surface function at equilibrium

Literature Cited

Adamczyk, Z., T. Babros, J. Czarnecki, and T. G. M. van de Ven, "Particle Transfer to Solid Surface," *Adv. Coll. Int. Sci.*, **19**, 183 (1983).

Andrade, J. D., "Principles of Protein Adsorption," *Surface and Interfacial Aspects of Biomolecular Polymers: 2. Protein Adsorption*, J. D. Andrade, ed., Plenum Press, New York (1985).

Bartelt, M. C., and V. Privman, "Kinetics of Irreversible Monolayer and Multilayer Adsorption," *Int. J. Mod. Phys. B*, **5**, 2883 (1991).

Ben-Avraham, D., "Lattice Models for Heterogeneous Catalysis," *Physica A*, **168**, 626 (1990).

Berninger, J. A., R. D. Whitley, X. Zhang, and N.-H. L. Wang, "The Versatile Model for Simulation of Reaction and Non-Equilibrium Dynamics in Multicomponent Fixed-Bed Adsorption Processes," *Computers Chem. Eng.*, **15**, 749 (1991).

Berryman, J. B., "Random Close Packing of Hard Spheres and Disks," *Phys. Rev. A*, **27**, 1053 (1983).

Brunauer, S., P. H. Emmett, and E. Teller, "Adsorption of Gases in Multimolecular Layers," *J. Am. Chem. Soc.*, **60**, 309 (1938).

Brynda, E., M. Houska, and F. Lednicky, "Adsorption of Human Fibrinogen onto Hydrophobic Surfaces: The Effect of Concentration in Solution," *J. Colloid and Interf. Sci.*, **113**, 163 (1986).

Cary, N. C., "SAS/ETS User's Guide," Version 6, SAS Inst. (1988).

Cuypers, P. A., "Dynamic Ellipsometry: Biochemical and Biomedical Applications," PhD Thesis, Univ. of Limburg, Maastricht, Netherlands (1976).

Evans, J. W., "Random and Cooperative Sequential Adsorption," *Rev. Mod. Phys.*, **65**, 1281 (1993).

Feder, J., and I. Giaever, "Adsorption of Ferritin," *J. Colloid Int. Sci.*, **78**, 144 (1980a).

Feder, J., "Random Sequential Adsorption," *Theor. Biol.*, **87**, 237 (1980b).

Fowler, R. H., and E. A. Guggenhein, *Statistical Thermodynamics. Statistical Mechanics for Students of Physics and Chemistry*, Macmillan, New York (1939).

Freundlich, H., *Colloid and Capillary Chemistry*, Mathuen, London, p. 110 (1926).

Fritz, W., and E. U. Schlunder, "Simultaneous Adsorption Equilibria of Organic Solutes in Dilute Aqueous Solutions on Activated Carbon," *Chem. Eng. Sci.*, **29**, 1279 (1974).

Glessner, A. J., and A. L. Myers, "Sorption of Gas Mixtures in Molecular Sieves," *AIChE Symp. Ser.*, **65**, 73 (1969).

Henderson, D., "Single Equation of State for Hard Disks," *Mol. Phys.*, **30**, 971 (1975).

Honig, J. M., and L. H. Reyerson, "Adsorption of Nitrogen, Oxygen, and Argon on Rutile at Low Temperatures; Applicability of the Concept of Surface Heterogeneity," *J. Phys. Chem.*, **56**, 140 (1952).

Jin, X., N.-H. L. Wang, G. Tarjus, and J. Talbot, "Irreversible Adsorption on Nonuniform Surfaces: the Random Site Model," *J. Phys. Chem.*, **97**, 4256 (1993).
Jolles, P., and J. Jolles, "What's New in Lysozyme Research?" *Mol. Cellular Biochem.*, **63**, 165 (1984).
Kop, J. M. M., P. A. Cuypers, T. Lindhout, H. C. Hemker, and W. Th. Hermens, "The Adsorption of Prothrombin to Phospholipid Monolayers Quantitated by Ellipsometry," *J. Biol. Chem.*, **259**, 13993 (1984).
Kopaciewicz, W., M. A. Rounds, J. Fausnaugh, and F. E. Regnier, "Retention Model for High-Performance Ion-Exchange Chromatography," *J. Chromatog*, **266**, 3 (1983).
Langmuir, I., "The Adsorption of Gases on Plane Surface of Glass, Mica and Platinum," *J. Chem. Soc.*, **40**, 1361 (1918).
Leininger, R. I., T. B. Hutson, and R. J. Jakobsen, "Spectroscopic Approaches to the Investigation of Interactions between Artificial Surfaces and Proteins," *Annals New York Academy of Sciences*, **516**, 173 (1987).
Lundstrom, I., "Surface Physics and Biological Phenomena," *Phys. Scr.*, **T4**, 5 (1983).
Mao, Q. M., A. Johnston, I. G. Prince, and M. T. W. Hearn, "High-Performance Liquid Chromatography of Amino Acids, Peptides and Proteins: CXIII, Predicting the Performance of Non-porous Particles in Affinity Chromatography of Proteins," *J. Chromatog.*, **548**, 147 (1991).
Markham, E. C., and A. F. Benton, "The Adsorption of Gas Mixtures by Silica," *J. Am. Chem. Soc.*, **53**, 497 (1931).
Myers, A. L., and J. M. Prausnitz, "Thermodynamics of Mixed-Gas Adsorption," *AIChE J.*, **11**, 121 (1965).
Nakahara, T., M. Hirata, and T. Omori, "Adsorption of Hydrocarbons on a Carbon Molecular Sieve," *J. Chem. Eng. Data*, **19**, 310 (1974).
Onoda, G. Y., and E. G. Liniger, "Experimental Determination of the Random-Parking Limit in Two Dimensions," *Phys. Rev. A*, **33**, 715 (1986).
Pomeau, Y., "Some Asymptotic Estimates in Random Parking Problem," *J. Phys. A*, **13**, L193 (1980).
Privman, V., J. S. Wang, and P. Nielaba, "Continuum Limit in Random Sequential Adsorption," *Phys. Rev. B*, **43**, 3366 (1991).
Radke, C. J., and J. M. Prausnitz, "Thermodynamics of Multisolute Adsorption from Dilute Liquid Solutions," *AIChE J.*, **18**, 761 (1972).
Ramsden, J. J., "Observation of Anomolous Diffusion of Proteins near Surfaces," *J. Phys. Chem.*, **96**, 3388 (1992).
Ramsden, J. J., "Concentration Scaling of Protein Deposition Kinetics," *Phys. Rev. Lett.*, **71**, 295 (1993).
Regnier, F. E., "High-performance Liquid Chromatography of Biopolymers," *Sci.*, **222**, 245 (1983).
Rounds, M. A. and F. E. Regnier, "Evaluation of a Retention Model for High-Performance Ion-Exchange Chromatography Using Two Different Displacing Salts," *J. Chromatog.*, **283**, 37 (1984).
Scatchard, G., "The Attraction of Proteins for Small Molecules and Ions," *Ann. N.Y. Acad. Sci.*, **51**, 660 (1949).
Schaaf, P., and J. Talbot, "Kinetics of Random Sequential Adsorption," *Phys. Rev. Lett.*, **62**, 175 (1989a).
Schaaf, P., and J. Talbot, "Surface Exclusion Effects in Adsorption Processes," *J. Chem. Phys.*, **91**, 4401 (1989b).
Scope, R. K., *Protein Purification*, Springer-Verlag, New York (1982).
Skidmore, G. L., B. J. Horstmann, and H. A. Chase, "Modeling Single-Component Protein Adsorption on the Cation Exchanger S Sepharose FF," *J. Chromatog.*, **498**, 113 (1990).
Swendsen, R. H., "Dynamics of Random Sequential Adsorption," *Phys. Rev. A*, **24**, 504 (1981).
Szepesy, L., and V. Illes, "Adsorption of Hases and Gas Mixtures: II. Measurement of the Adsorption Isotherms of Gases on Active Carbon under Pressures of 1 to 7 atm," *Acta Chim. Acad. Sci. Hung.*, **35**, 53 (1963).
Tarjus, G., P. Schaaf, and J. Talbot, "Generalized Random Sequential Adsorption," *J. Chem. Phys.*, **93**, 8352 (1990).
Tiefenthaler, K., and W. Lukosz, "Sensitivity of Grating Couples as Integrated-Optical Chemical Sensors," *J. Opt. Soc. Am. B: Opt. Phys.*, **6**, 209 (1989).
Toth, J., "State Equations of the Solid-Gas Interface Layers," *Acta Chim. Acad. Sci. Hung.*, **69**, 311 (1971).
Valenzuela, D. P., and A. L. Myers, *Adsorption Equilibrium Data Handbook*, Prentice Hall, New York (1989).
Wankat, P. C., *Rate-Controlled Separations*, Elsevier Applied Science, New York (1990).
Widom, B., "Random Sequential Addition of Hard Spheres to a Volume," *J. Chem. Phys.*, **44**, 3888 (1966).

Manuscript received Oct. 4, 1993, and revision received Dec. 3, 1993.